Augmented Roe Solver for hydrodynamic shallow flows

S. Martínez-Aranda*

Peka2D-v5 Doc – Fluid Dynamic Technologies-I3A, University of Zaragoza, Spain

Abstract

Keywords:

1. Governing equations

The depth-averaged 2D model for the hydrodynamic shallow flows involves the continuity equations for the flow volume, rewritten here as

$$\frac{\partial(h)}{\partial t} + \frac{\partial}{\partial x}(hu) + \frac{\partial}{\partial y}(hv) = r - i \tag{1}$$

and the conservation laws of the linear momentum along the $x-$ and $y-$coordinates, which can be expressed as

$$\frac{\partial(hu)}{\partial t} + \frac{\partial}{\partial x}(hu^2 + \frac{1}{2}g_\psi h^2) + \frac{\partial}{\partial y}(huv) = -g_\psi h\frac{\partial z_b}{\partial x} - \frac{\tau_{bx}}{\rho} \tag{2a}$$

$$\frac{\partial(hv)}{\partial t} + \frac{\partial}{\partial x}(huv) + \frac{\partial}{\partial y}(hv^2 + \frac{1}{2}g_\psi h^2) = -g_\psi h\frac{\partial z_b}{\partial x} - \frac{\tau_{by}}{\rho} \tag{2b}$$

being h the vertical flow depth and $\mathbf{u} = (u,\, v)$ the depth-averaged flow velocity vector, z_b the bed layer elevation, $\boldsymbol{\tau_b} = (\tau_{bx},\, \tau_{by})$ the depth-averaged basal resistance vector and ρ the flow density. The terms on the right hand side of the continuity equation account for the effective rainfall r and the infiltration rate i. It is worth noting that the dispersive terms on the right hand side have been neglected. The local bed-normal projection of the gravity has been used here to integrate the pressure and volumetric force terms, with $g_\psi = g\cos^2\psi$, being g the gravitational acceleration and ψ the bed-normal angle respect to the vertical axis [1].

*** Hay que implmentar la proyeccion de la gravedad g_ψ en el R-solver (water.cu) ***

The basal shear stress vector in the momentum equations (2) is expressed as

$$\boldsymbol{\tau_b} = (\tau_{bx}, \tau_{by}) = \tau_b\, \mathbf{n_u} \tag{3}$$

being $\mathbf{n_u} = (n_{ux}, n_{uy})$ the velocity unit vector and τ_b the basal shear stress modulus estimated by the turbulent Manning relation, written as

$$\tau_b = \rho g_\psi h \frac{n_b^2}{h^{4/3}} |\mathbf{u}|^2 \tag{4}$$

being n_b the Manning roughness parameter.

*Corresponding author

Email address: `sermar@unizar.es` (S. Martínez-Aranda)

The equations forming the system can be recast as five conservation laws and rewritten in vector form as

$$\frac{\partial \mathbf{U}}{\partial t} + \nabla \cdot \mathbf{E}(\mathbf{U}) = \mathbf{Q}(\mathbf{U}) + \mathbf{S_b}(\mathbf{U}) + \mathbf{S}_{\boldsymbol{\tau}}(\mathbf{U}) \tag{5}$$

where $\mathbf{U}$ is the vector of conserved variables

$$\mathbf{U} = \begin{pmatrix} h, & hu, & hv \end{pmatrix}^T \tag{6}$$

and $\mathbf{E}(\mathbf{U}) = \big(\mathbf{F}(\mathbf{U}), \mathbf{G}(\mathbf{U})\big)$ are the convective fluxes along the $\mathbf{X} = (x, y)$ horizontal coordinates respectively.

$$\mathbf{F}(\mathbf{U}) = \begin{pmatrix} hu \\ hu^2 + \frac{1}{2} g_\psi h^2 \\ huv \end{pmatrix} \quad \mathbf{G}(\mathbf{U}) = \begin{pmatrix} hv \\ huv \\ hv^2 + \frac{1}{2} g_\psi h^2 \end{pmatrix} \tag{7}$$

The vector $\mathbf{Q}(\mathbf{U})$ accounts for the mass source terms, whereas the vector $\mathbf{S_b}(\mathbf{U})$ and $\mathbf{S}_\tau(\mathbf{U})$ account for the momentum source term associated to the bed pressure and the frictional momentum dissipation.

$$\mathbf{Q}(\mathbf{U}) = \begin{pmatrix} r - i \\ 0 \\ 0 \end{pmatrix} \qquad \mathbf{S_b}(\mathbf{U}) = \begin{pmatrix} 0 \\ -g_\psi h \frac{\partial z_b}{\partial x} \\ -g_\psi h \frac{\partial z_b}{\partial y} \end{pmatrix} \qquad \mathbf{S}_{\boldsymbol{\tau}}(\mathbf{U}) = \begin{pmatrix} 0 \\ -\frac{\tau_b}{\rho} n_{ux} \\ -\frac{\tau_b}{\rho} n_{uy} \end{pmatrix} \tag{8}$$

2. Finite Volume method

System (5) is time dependent, non linear and contains mass and momentum source terms. It can be classified as belonging to the family of hyperbolic systems. In order to obtain a numerical solution, the spatial domain is divided in computational cells using a fixed-in-time mesh and system (5) is integrated in each cell Ω_i. Applying the Gauss theorem leads to

$$\frac{\mathrm{d}}{\mathrm{d}t} \int_{\Omega_i} \mathbf{U}\,\mathrm{d}\Omega + \oint_{\partial\Omega_i} \mathbf{E}(\mathbf{U}) \cdot \mathbf{n}\,\mathrm{d}l = \int_{\Omega_i} \mathbf{Q}(\mathbf{U})\,\mathrm{d}\Omega + \int_{\Omega_i} \mathbf{S_b}(\mathbf{U})\,\mathrm{d}\Omega + \int_{\Omega_i} \mathbf{S}_{\boldsymbol{\tau}}(\mathbf{U})\,\mathrm{d}\Omega \tag{9}$$

being $\mathbf{E}(\mathbf{U}) \cdot \mathbf{n}$ the normal flux and $\mathbf{n} = (n_x, n_y)$ the outward unit normal vector along the i cell boundary $\partial\Omega_i$. Assuming a piecewise uniform representation of the conserved variables $\mathbf{U}$ at the cell Ω_i, the integrated system (9) can be expressed as

$$\frac{\mathrm{d}}{\mathrm{d}t} \int_{\Omega_i} \mathbf{U}\,\mathrm{d}\Omega + \sum_{k=1}^{\mathrm{NE}} (\mathbf{E} \cdot \mathbf{n})_k\, l_k = \int_{\Omega_i} \mathbf{Q}(\mathbf{U})\,\mathrm{d}\Omega + \int_{\Omega_i} \mathbf{S_b}(\mathbf{U})\,\mathrm{d}\Omega + \int_{\Omega_i} \mathbf{S}_{\boldsymbol{\tau}}(\mathbf{U})\,\mathrm{d}\Omega \tag{10}$$

being NE the number of edges for the i cell, $(\mathbf{E} \cdot \mathbf{n})_k$ the value of the normal flux through the kth edge, l_k the length of the edge.

The left hand side of (5), the conservative flux matrix $\mathbf{E}(\mathbf{U})$ satisfies the rotation invariant property [2] since

$$\nabla \cdot \mathbf{E}(\mathbf{U}) = \mathbf{R}_k^{-1}\, \hat{\nabla} \cdot \mathbf{E}(\mathbf{R}_k \mathbf{U}) \tag{11}$$

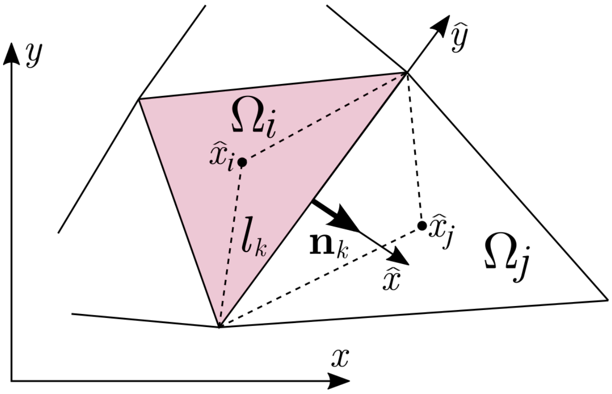

Figure 1: Local coordinates at the kth cell edge.

where $\hat{\nabla} = \boldsymbol{\mathcal{R}}_k \nabla$ and $\boldsymbol{\mathcal{R}}_k$ is a 2×2 rotation matrix which projects the global orthogonal coordinates $\mathbf{X} = (x, y)$ into the local framework $\hat{\mathbf{X}} = \boldsymbol{\mathcal{R}}_k \mathbf{X} = (\hat{x}, \hat{y})$, being $\hat{x}$ and $\hat{y}$ the normal and the tangential coordinate to the kth cell edge respectively (Figure 1):

$$\boldsymbol{\mathcal{R}}_k = \begin{pmatrix} \mathbf{n} \\ \mathbf{t} \end{pmatrix}_k = \begin{pmatrix} n_x & n_y \\ -n_y & n_x \end{pmatrix}_k \tag{12}$$

where $\mathbf{n} = (n_x, n_y)$ and $\mathbf{t} = (-n_y, n_x)$ are the normal and tangential unit vectors respectively. The complete 3×3 rotation matrix $\mathbf{R}_k$ in (11) and its inverse $\mathbf{R}_k^{-1}$ for the kth cell edge are defined as

$$\begin{aligned} \mathbf{R}_k &= \left(\begin{array}{c|c} 1 & \\ \hline & \boldsymbol{\mathcal{R}} \end{array}\right)_k = \begin{pmatrix} 1 & 0 & 0 \\ 0 & n_x & n_y \\ 0 & -n_y & n_x \end{pmatrix}_k \\ \mathbf{R}_k^{-1} &= \left(\begin{array}{c|c} 1 & \\ \hline & \boldsymbol{\mathcal{R}}^{-1} \end{array}\right)_k = \begin{pmatrix} 1 & 0 & 0 \\ 0 & n_x & -n_y \\ 0 & n_y & n_x \end{pmatrix}_k \end{aligned} \tag{13}$$

and the convective flux term in (10) satisfies the condition [3]

$$(\mathbf{E} \cdot \mathbf{n})_k = \Big[\mathbf{F}(\mathbf{U})\, n_x + \mathbf{G}(\mathbf{U})\, n_y\Big]_k = \mathbf{R}_k^{-1}\, \mathbf{F}(\mathbf{R}_k \mathbf{U}) \tag{14}$$

Using (14), the homogeneous left hand side of (10) can be expressed as

$$\frac{\mathrm{d}}{\mathrm{d}t} \int_{\Omega_i} \mathbf{U}\, \mathrm{d}\Omega + \sum_{k=1}^{\mathrm{NE}} \mathbf{R}_k^{-1}\, \mathbf{F}(\hat{\mathbf{U}})_k\, l_k \tag{15}$$

where $\hat{\mathbf{U}} \equiv \mathbf{R}_k \mathbf{U}$ and $\mathbf{F}(\hat{\mathbf{U}})_k \equiv \mathbf{F}(\mathbf{R}_k \mathbf{U})$ denote respectively the set of local conservative variables and the conservative flux vector at the cell edge, defined as

$$\hat{\mathbf{U}} \equiv \mathbf{R}_k \mathbf{U} = \begin{pmatrix} h \\ hu_n \\ hv_t \end{pmatrix} \qquad \mathbf{F}(\hat{\mathbf{U}})_k \equiv \mathbf{F}(\mathbf{R}_k \mathbf{U}) = \begin{pmatrix} hu_n \\ hu_n^2 + \frac{1}{2} g_\psi h^2 \\ hu_n v_t \end{pmatrix} = \begin{pmatrix} q_n \\ m_n \\ m_t \end{pmatrix} \tag{16}$$

being $u_n = u n_x + v n_y$ and $v_t = -u n_y + v n_x$ the components of the flow velocity in the local framework $\hat{\mathbf{u}} = \boldsymbol{\mathcal{R}}_k \mathbf{u}$. We denote as q_n the mass flux normal to the cell edge, and m_n and m_t the momentum flux normal and tangential to the cell edge respectively.

The value of the fluxes through the kth cell edge can be augmented incorporating the non-conservative contribution of the momentum source terms $\mathbf{S_b}$ and $\mathbf{S}_{\boldsymbol{\tau}}$ into the homogeneous normal fluxes $\mathbf{F}(\hat{\mathbf{U}})_k$ [4]. The bed-pressure term $\mathbf{S_b}$ is unconditionally invariant under rotation [5] and can be included within the local framework $(\hat{x}, \hat{y})$ using the spatial discretization

$$\int_{\Omega_i} \mathbf{S_b}(\mathbf{U})\, \mathrm{d}\Omega = \sum_{k=1}^{\mathrm{NE}} \mathbf{R}_k^{-1}\, \mathbf{H}(\hat{\mathbf{U}})_k\, l_k \tag{17}$$

where

$$\mathbf{H}(\hat{\mathbf{U}})_k = \begin{pmatrix} 0 \\ -g_\psi\, h\, \Delta z_b \\ 0 \end{pmatrix} \tag{18}$$

is the integrated bed pressure at the kth cell edge [6] expressed in the local framework (see Section 2.4).

The spatial discretization of the basal resistance integral is open to different possibilities since, contrarily to bed-pressure momentum source contribution, the maintenance of the rotation invariant property is not straightforward for the 2D shear stresses. The upwind discretization of the 2D basal resistance term allows to rewrite the cell-centered integral of the the basal shear stress as a sum of edge-contributions

$$\int_{\Omega_i} \mathbf{S}_{\boldsymbol{\tau}}(\mathbf{U})\, \mathrm{d}\Omega = \sum_{k=1}^{\mathrm{NE}} \mathbf{R}_k^{-1}\, \mathbf{T}(\hat{\mathbf{U}})_k\, l_k \tag{19}$$

where $\mathbf{T}(\hat{\mathbf{U}})_k$ is the integrated basal resistance throughout the kth cell edge, expressed in the local framework using a differential approach (Figure 2) as

$$\mathbf{T}(\hat{\mathbf{U}})_k = \begin{pmatrix} 0 \\ -\frac{\tau_b}{\rho}\, \mathbf{n_u} \cdot \mathbf{d_c} \\ 0 \end{pmatrix}_k \tag{20}$$

with $\mathbf{n_u} = (n_{ux}, n_{uy})$ velocity direction vector and $\mathbf{d_c} = (\Delta x, \Delta y)$ the space-vector between cell centres in the global coordinate system, due to the rotation invariance of the scalar product $\mathbf{n_u} \cdot \mathbf{d_c} = (\boldsymbol{\mathcal{R}}_k \mathbf{n_u}) \cdot (\boldsymbol{\mathcal{R}}_k \mathbf{d_c})$ [2].

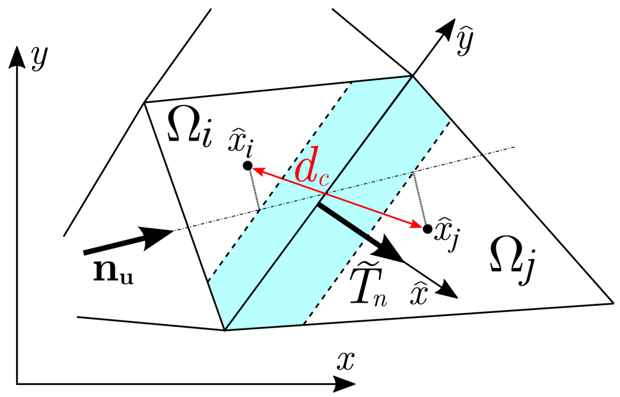

Figure 2: Differential procedure for the integration of the 2D resistance force.

Using (17) and (19), the local homogenous equation (15) can be augmented with the momentum source contributions as

$$\frac{\mathrm{d}}{\mathrm{dt}} \int_{\Omega_i} \mathbf{U}\, \mathrm{d}\Omega = -\sum_{k=1}^{\mathrm{NE}} \mathbf{R}_k^{-1} \left[\mathbf{F}(\hat{\mathbf{U}}) - \mathbf{H}(\hat{\mathbf{U}}) - \mathbf{T}(\hat{\mathbf{U}}) \right]_k l_k \tag{21}$$

allowing to define an augmented numerical flux $\boldsymbol{\mathcal{F}}_k^{\downarrow}$ for the kth cell edge defined as

$$\boldsymbol{\mathcal{F}}_k^{\downarrow} = \left[\mathbf{F}(\hat{\mathbf{U}}) - \mathbf{H}(\hat{\mathbf{U}}) - \mathbf{T}(\hat{\mathbf{U}}) \right]_k \tag{22}$$

Furthermore, the hydrological term $\mathbf{Q}(\mathbf{U})$ accounts for a flow volume source/sink and hence its nature is different from the other source terms on the right hand side of (10). For the sake of simplicity, it is discretized in space as

$$\int_{\Omega_i} \mathbf{Q}(\mathbf{U})\, d\Omega \approx A_i\, \mathbf{Q}(\mathbf{U}_i) = A_i\, \boldsymbol{\mathcal{Q}}_i \tag{23}$$

where A_i id the discrete cell area, and the resulting integrated system (10) can be expressed as

$$\frac{\mathrm{d}}{\mathrm{dt}} \int_{\Omega_i} \mathbf{U}\, \mathrm{d}\Omega = -\sum_{k=1}^{\mathrm{NE}} \mathbf{R}_k^{-1}\, \boldsymbol{\mathcal{F}}_k^{\downarrow}\, l_k + A_i\, \boldsymbol{\mathcal{Q}}_i \tag{24}$$

Assuming a piecewise uniform representation of the conserved variables $\mathbf{U}$ at the i cell for the time $t = t^n$

$$\mathbf{U}_i^n = \frac{1}{A_i} \int_{\Omega_i} \mathbf{U}(x, y, t^n)\, \mathrm{d}\Omega \tag{25}$$

and using explicit temporal integration for the mass and momentum source terms, the updating formulation for the conserved variables $\mathbf{U}$ at the each cell is expressed as

$$\mathbf{U}_i^{n+1} = \mathbf{U}_i^n - \frac{\Delta t}{A_i} \sum_{k=1}^{\mathrm{NE}} \mathbf{R}_k^{-1}\, \boldsymbol{\mathcal{F}}_k^{\downarrow}\, l_k + \Delta t\, \boldsymbol{\mathcal{Q}}_i^n \tag{26}$$

being $\Delta t = t^{n+1} - t^n$ the time step. Hence the resolution procedure needs to compute the numerical fluxes $\boldsymbol{\mathcal{F}}_k^{\downarrow}$ at the cell edges.

This updating formula also admits a flux-contribution version by considering that the flux vector at the intercell edge $\boldsymbol{\mathcal{F}}_k^{\downarrow}$ can be rewritten as $\boldsymbol{\mathcal{F}}_k^{\downarrow} = \mathbf{F}(\mathbf{R}_k \mathbf{U}_i) + \boldsymbol{\delta\mathcal{F}}_k^{\downarrow}$, where the term $\boldsymbol{\delta\mathcal{F}}_k^{\downarrow}$ accounts for the flux step between the cell center and the intercell edge. Considering that $\sum_{k=1}^{\mathrm{NE}} \mathbf{R}_k^{-1}\, \mathbf{F}(\mathbf{R}_k \mathbf{U}_i) = 0$, the flux-contribution version of the updating equation (26) can be expressed as:

$$\mathbf{U}_i^{n+1} = \mathbf{U}_i^n - \frac{\Delta t}{A_i} \sum_{k=1}^{\mathrm{NE}} \mathbf{R}_k^{-1}\, \boldsymbol{\delta\mathcal{F}}_k^{\downarrow}\, l_k + \Delta t\, \boldsymbol{\mathcal{Q}}_i^n \tag{27}$$

2.1. Augmented Riemann solver for hydrodynamic flows

The augmented numerical flux $\boldsymbol{\mathcal{F}}_k^{\downarrow}$ in the local framework $\hat{\mathbf{X}} = (\hat{x}, \hat{y})$ of the kth edge, separating the left i cell and the right j cell, can be computed as the approximate solution of a constant-coefficient linear Riemann problem (RP) [3] defined as

$$
\begin{aligned}
&\frac{\partial \hat{\mathbf{U}}}{\partial t} + \widetilde{\mathbf{J}}_k \frac{\partial \hat{\mathbf{U}}}{\partial \hat{x}} = \hat{\mathbf{S}}_{\mathbf{b}} + \hat{\mathbf{S}}_{\boldsymbol{\tau}} \\
&\hat{\mathbf{U}}(\hat{x},0) = \begin{cases} \hat{\mathbf{U}}_i = \mathbf{R}_k \mathbf{U}_i^n & \text{if} \quad \hat{x} < 0 \\ \hat{\mathbf{U}}_j = \mathbf{R}_k \mathbf{U}_j^n & \text{if} \quad \hat{x} > 0 \end{cases}
\end{aligned}
\tag{28}
$$

where $\widetilde{\mathbf{J}}_k = \widetilde{\mathbf{J}}_k(\hat{\mathbf{U}}_i, \hat{\mathbf{U}}_j)$ is a constant coefficient matrix which locally approximates the Jacobian of the non-linear RP, whereas $\hat{\mathbf{S}}_{\mathbf{b}}$ and $\hat{\mathbf{S}}_{\boldsymbol{\tau}}$ are the bed-pressure and basal resistance source terms in the local framework.

Integrating the homogeneous left hand side of (28) over the discrete space $\hat{x}_i \leq \hat{x} \leq \hat{x}_j$ leads to the following constraint involving conservation across discontinuities

$$
\boldsymbol{\delta}\mathbf{F}_k = \widetilde{\mathbf{J}}_k \, \boldsymbol{\delta}\hat{\mathbf{U}}_k \tag{29}
$$

where $\boldsymbol{\delta}\hat{\mathbf{U}}_k = \hat{\mathbf{U}}_j - \hat{\mathbf{U}}_i$ and $\boldsymbol{\delta}\mathbf{F}_k = \mathbf{F}(\hat{\mathbf{U}}_j) - \mathbf{F}(\hat{\mathbf{U}}_i)$ are the conserved variables and the homogeneous fluxes increment at the kth edge, respectively.

Using the Roe strategy [3], the approximate Jacobian $\widetilde{\mathbf{J}}_k$ reduces to a 3×3 constant matrix defined as

$$
\widetilde{\mathbf{J}}_k = \begin{pmatrix} 0 & 1 & 0 \\ g_\psi \widetilde{h} - \widetilde{u}_n^2 & 2\widetilde{u}_n & 0 \\ -\widetilde{u}_n \, \widetilde{v}_t & \widetilde{v}_t & \widetilde{u}_n \end{pmatrix}_k \tag{30}
$$

which satisfies (29) with the wall-averaged quantities

$$
\widetilde{h} = \frac{h_i + h_j}{2} \tag{31a}
$$

$$
\widetilde{u}_n = \frac{u_{ni}\sqrt{h_i} + u_{nj}\sqrt{h_j}}{\sqrt{h_i} + \sqrt{h_j}} \tag{31b}
$$

$$
\widetilde{v}_t = \frac{v_{ti}\sqrt{h_i} + v_{tj}\sqrt{h_j}}{\sqrt{h_i} + \sqrt{h_j}} \tag{31c}
$$

The approximate matrix $\widetilde{\mathbf{J}}_k$ (30) is diagonalizable with four real eigenvalues

$$
(\widetilde{\lambda}_1)_k = (\widetilde{u}_n - \widetilde{c})_k \qquad (\widetilde{\lambda}_2)_k = (\widetilde{u}_n)_k \qquad (\widetilde{\lambda}_3)_k = (\widetilde{u}_n + \widetilde{c})_k \tag{32}
$$

where the averaged wave-celerity is $\widetilde{c}_k = \sqrt{(g_\psi \widetilde{h})_k}$. Using the properties of the Jacobian, it is possible to build a matrix $\widetilde{\mathbf{P}}_k = (\widetilde{\mathbf{e}}_1, \widetilde{\mathbf{e}}_2, \widetilde{\mathbf{e}}_3)_k$ which satisfies $\widetilde{\mathbf{J}}_k = (\widetilde{\mathbf{P}}\widetilde{\boldsymbol{\Lambda}}\widetilde{\mathbf{P}}^{-1})_k$, being $\widetilde{\boldsymbol{\Lambda}}_k$ the diagonal eigenvalues matrix and $(\widetilde{\mathbf{e}}_m)_k$ the orthogonal basis of eigenvectors, defined as

$$
(\widetilde{\mathbf{e}}_1)_k = \begin{pmatrix} 1 \\ \widetilde{\lambda}_1 \\ \widetilde{v}_t \end{pmatrix}_k \qquad (\widetilde{\mathbf{e}}_2)_k = \begin{pmatrix} 0 \\ 0 \\ \widetilde{c} \end{pmatrix}_k \qquad (\widetilde{\mathbf{e}}_3)_k = \begin{pmatrix} 1 \\ \widetilde{\lambda}_3 \\ \widetilde{v}_t \end{pmatrix}_k \tag{33}
$$

Following [3], the conservative variable gradient $\boldsymbol{\delta}\hat{\mathbf{U}}_k$ is projected on the eigenvector basis in order to obtain the wave strength vectors $\widetilde{\mathbf{A}}_k$ as

$$
\widetilde{\mathbf{A}}_k = (\widetilde{\alpha}_1, \, \widetilde{\alpha}_2, \, \widetilde{\alpha}_3)_k^T = \widetilde{\mathbf{P}}_k^{-\mathbf{1}} \, \boldsymbol{\delta}\hat{\mathbf{U}}_k \quad \longrightarrow \quad \boldsymbol{\delta}\hat{\mathbf{U}}_k = \sum_m (\widetilde{\alpha}_w \widetilde{\mathbf{e}}_w)_k \tag{34}
$$

being

$$\begin{aligned}
\widetilde{\alpha}_1 &= \frac{1}{2}\delta(h) - \frac{1}{2}\frac{\delta(hu_n) - \widetilde{u}_n\,\delta(h)}{\widetilde{c}} \\
\widetilde{\alpha}_2 &= \frac{\delta(hv_t) - \widetilde{v}_t\,\delta(h)}{\widetilde{c}} \\
\widetilde{\alpha}_3 &= \frac{1}{2}\delta(h) + \frac{1}{2}\frac{\delta(hu_n) - \widetilde{u}_n\,\delta(h)}{\widetilde{c}}
\end{aligned} \tag{35}$$

The bed-pressure and basal resistance momentun source terms on the right hand side of (28) are integrated over the discrete space $\hat{x}_i \leq \hat{x} \leq \hat{x}_j$ as

$$\int_{\hat{x}_i}^{\hat{x}_j} \hat{\mathbf{S}}_{\mathbf{b}}\,\mathrm{d}\hat{x} = \mathbf{H}(\hat{\mathbf{U}}_i, \hat{\mathbf{U}}_j) = \mathbf{H}_k = (0, \widetilde{H}, 0)_k^T \tag{36a}$$

$$\int_{\hat{x}_i}^{\hat{x}_j} \hat{\mathbf{S}}_{\boldsymbol{\tau}}\,\mathrm{d}\hat{x} = \mathbf{T}(\hat{\mathbf{U}}_i, \hat{\mathbf{U}}_j) = \mathbf{T}_k = (0, \widetilde{T}, 0)_k^T \tag{36b}$$

and these momentum edge-contributions can be projected on the eigenvector basis in order to obtain the source strength vectors as

$$(\widetilde{\mathbf{B}}_{\mathbf{b}})_k = (\widetilde{\beta}_{b1},\, \widetilde{\beta}_{b2},\, \widetilde{\beta}_{b3})_k^T = \widetilde{\mathbf{P}}_k^{-1}\,\mathbf{H}_k \quad \longrightarrow \quad \mathbf{H}_k = \sum_m (\widetilde{\beta}_{bm}\widetilde{\mathbf{e}}_w)_k \tag{37a}$$

$$(\widetilde{\mathbf{B}}_{\boldsymbol{\tau}})_k = (\widetilde{\beta}_{\tau 1},\, \widetilde{\beta}_{\tau 2},\, \widetilde{\beta}_{\tau 3})_k^T = \widetilde{\mathbf{P}}_k^{-1}\,\mathbf{T}_k \quad \longrightarrow \quad \mathbf{T}_k = \sum_m (\widetilde{\beta}_{\tau m}\widetilde{\mathbf{e}}_w)_k \tag{37b}$$

and the total source strength reads

$$\widetilde{\mathbf{B}}_k = (\widetilde{\beta}_1,\, \widetilde{\beta}_1,\, \widetilde{\beta}_4)_k^T = (\widetilde{\mathbf{B}}_{\mathbf{b}} + \widetilde{\mathbf{B}}_{\boldsymbol{\tau}})_k \tag{38}$$

leading to

$$\begin{aligned}
\widetilde{\beta}_1 &= \frac{-1}{2}\frac{\widetilde{H} + \widetilde{T}}{\widetilde{c}} \\
\widetilde{\beta}_2 &= 0 \\
\widetilde{\beta}_3 &= \frac{1}{2}\frac{\widetilde{H} + \widetilde{T}}{\widetilde{c}}
\end{aligned} \tag{39}$$

Note that this procedure allows to include the upwind contribution of the real 2D bed-pressure and basal resistance source terms into the plane RP at the cell edges. The integration of both contributions at the cell edges are detailed in sections 2.4 and 2.5 respectively.

One result of Roe's linearization is that the approximate Riemann solution consists of only discontinuities and hence $\hat{\mathbf{U}}(\hat{x}, t)$ is constructed as a sum of discontinuities or shocks. Figure 3 shows the wave structure of the approximate solution for subcritical and supercritical flow regimes. Using (35) and (38), the intermediate states (blue regions) of the approximate solution at the left and right side of the kth edge, $\hat{\mathbf{U}}_i^-$ and $\hat{\mathbf{U}}_j^+$ respectively, can be expressed as

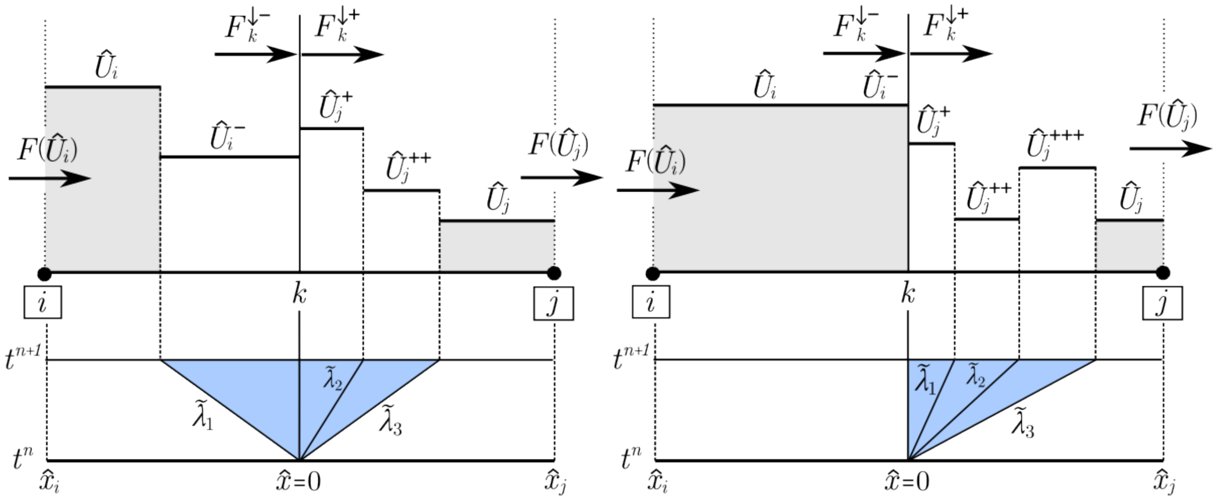

Figure 3: Approximate solution at the kth cell edge for (left) subcritical and (right) supercritical regime.

$$\begin{aligned}
\hat{\mathbf{U}}_i^- &= \hat{\mathbf{U}}_i + \sum_{w-} \left[\left(\widetilde{\alpha}_w - \widetilde{\beta}_w/\widetilde{\lambda}_w\right) \widetilde{\mathbf{e}}_w \right]_k \\
\hat{\mathbf{U}}_j^+ &= \hat{\mathbf{U}}_j - \sum_{w+} \left[\left(\widetilde{\alpha}_w - \widetilde{\beta}_w/\widetilde{\lambda}_w\right) \widetilde{\mathbf{e}}_w \right]_k
\end{aligned} \tag{40}$$

where the subscript $m-$ and $m+$ under the sums indicate waves travelling inward and outward the i cell [4]. Note that at $\hat{x} = 0$ the solution includes a steady discontinuity between the intermediate states $\hat{\mathbf{U}}_i^-$ and $\hat{\mathbf{U}}_j^+$ [7, 8] as a consequence of including the momentum source terms into the local plane RP. This steady shock can be expressed as

$$\hat{\mathbf{U}}_j^+ - \hat{\mathbf{U}}_i^- = \sum_{w=1}^{3} \left(\frac{\widetilde{\beta}_w}{\widetilde{\lambda}_w} \widetilde{\mathbf{e}}_w \right)_k \tag{41}$$

Consequently, the augmented flux at the left and right side of the kth cell edge, $\boldsymbol{\mathcal{F}}_k^{\downarrow -}$ and $\boldsymbol{\mathcal{F}}_k^{\downarrow +}$ respectively, can be constructed as

$$\begin{aligned}
\boldsymbol{\mathcal{F}}_k^{\downarrow -} &= \mathbf{F}(\hat{\mathbf{U}}_i) + \sum_{w-} \left[\left(\widetilde{\lambda}_w \widetilde{\alpha}_w - \widetilde{\beta}_w\right) \widetilde{\mathbf{e}}_w \right]_k \\
\boldsymbol{\mathcal{F}}_k^{\downarrow +} &= \mathbf{F}(\hat{\mathbf{U}}_j) - \sum_{w+} \left[\left(\widetilde{\lambda}_w \widetilde{\alpha}_w - \widetilde{\beta}_w\right) \widetilde{\mathbf{e}}_w \right]_k
\end{aligned} \tag{42}$$

where the subscript $m-$ and $m+$ under the sums indicate waves travelling inward and outward the i cell. The relation between the approximate fluxes $\boldsymbol{\mathcal{F}}_k^{\downarrow -}$ and $\boldsymbol{\mathcal{F}}_k^{\downarrow +}$ can be analysed using the Rankine-Hugoniot (RH) relation at $\hat{x} = 0$, which includes the steady contact wave accounting for the momentum sources. The corresponding flux discontinuity is given by

$$\boldsymbol{\mathcal{F}}_k^{\downarrow +} - \boldsymbol{\mathcal{F}}_k^{\downarrow -} = \sum_{w=1}^{3} (\widetilde{\beta}_w \widetilde{\mathbf{e}}_w)_k = \mathbf{H}_k + \mathbf{T}_k \tag{43}$$

Therefore, the numerical flux vector $\boldsymbol{\mathcal{F}}_k^{\downarrow}$ in the updating formula (26) of the FV method is upwind computed as

$$\boldsymbol{\mathcal{F}}_k^{\downarrow} \equiv \boldsymbol{\mathcal{F}}_k^{\downarrow-} = \begin{bmatrix} q_n \\ m_n \\ m_t \end{bmatrix}_k^{\downarrow-} \tag{44}$$

whereas the flux-contribution in the updating formula (27) can also be upwind calculated as

$$\boldsymbol{\delta\mathcal{F}}_k^{\downarrow} \equiv \boldsymbol{\delta\mathcal{F}}_k^{\downarrow-} = \sum_{w-} \left[(\widetilde{\lambda}_w \widetilde{\alpha}_w - \widetilde{\beta}_w) \widetilde{\mathbf{e}}_w \right]_k = \begin{bmatrix} \delta q_n \\ \delta m_n \\ \delta m_t \end{bmatrix}_k^{\downarrow-} \tag{45}$$

2.2. Entropy correction in transcritical rarefactions

To avoid non-physical result in walls involving transonic rarefactions, an improved version of the the Harten-Hyman entropy correction [9] is implemented.

The eigenvalues at the left i and right j cells at the kth edge are defined as

$$(\lambda_1)_{i,j} = (u_n - c)_{i,j} \qquad (\lambda_2)_{i,j} = (u_n)_{i,j} \qquad (\lambda_3)_{i,j} = (u_n + c)_{i,j} \tag{46}$$

Only for **wet-wet subcritical walls**, i.e. $(\widetilde{\lambda}_1)_k < 0$ & $(\widetilde{\lambda}_3)_k > 0$, the entropy fix is implemented as follows

- Left transcritical rarefaction $(\lambda_1)_i < 0$ & $(\lambda_1)_j > 0$

$$\begin{aligned} ECF &= \frac{(\lambda_1)_j - (\widetilde{\lambda}_1)_k}{(\lambda_1)_j - (\lambda_1)_i} (\lambda_1)_i < 0 \\ (\widetilde{\lambda}_1^-)_k &= ECF \rightarrow \text{new } (\widetilde{\lambda}_1)_k \\ (\widetilde{\lambda}_1^+)_k &= (\widetilde{\lambda}_1)_k - ECF \end{aligned} \tag{47}$$

- Right transcritical rarefaction $(\lambda_3)_i < 0$ & $(\lambda_3)_j > 0$

$$\begin{aligned} ECF &= \frac{(\widetilde{\lambda}_3)_k - (\lambda_3)_i}{(\lambda_3)_j - (\lambda_3)_i} (\lambda_3)_j > 0 \\ (\widetilde{\lambda}_3^-)_k &= (\widetilde{\lambda}_3)_k - ECF \\ (\widetilde{\lambda}_3^+)_k &= ECF \rightarrow \text{new } (\widetilde{\lambda}_3)_k \end{aligned} \tag{48}$$

2.3. Dynamic time step restriction

In order to ensure the stability of the explicitly computed numerical solution, the time step should be small enough to avoid the interaction of waves from neighbouring Riemann problems. The dynamical limitation of the time step at each k edge is addressed here assuming that the fastest wave celerity corresponds to the absolute maximum of the eigenvalues of $\widetilde{\mathbf{J}}_k$ (30) as

$$\Delta t_k = \frac{\min(A_i, A_j)}{l_k \left[\max(|\widetilde{\lambda}_1|, |\widetilde{\lambda}_3|) \right]_k} \tag{49}$$

*** Hay que cambiar el calculo de $\Delta\mathcal{X}_k$ en el codigo (mesh.c) ***

and the global time step $\Delta t = t^{n+1} - t^n$ is limited using the Courant-Friedrichs-Lewy (CFL) condition

$$\Delta t = \text{CFL} \min_k (\Delta t_k) \tag{50}$$

with CFL < 0.5 for square orthogonal meshes and CFL < 1 for the triangular mesh topology and 1D-mesh cases.

2.4. Bed pressure momentum contribution

The bed pressure contribution $\widetilde{H}_k$ at the kth cell edge in (39) is computed here as

$$\widetilde{H}_k = \begin{cases} \widetilde{H}^{int} & \text{default} \\ \max(\widetilde{H}^{int}, \widetilde{H}^{dif}) & \text{if } (\widetilde{u}_n \, \Delta z_b) > 0 \text{ and } (\Delta z_s \, \Delta z_b) > 0 \end{cases} \tag{51}$$

being

- Integral approximation:

$$\widetilde{H}^{int} = -g_\psi \left(h^* - \frac{|\delta z^*|}{2} \right) \delta z^*$$
$$h^* = \begin{cases} h_i & \text{if } \Delta z_b < 0 \\ h_j & \text{if } \Delta z_b \geq 0 \end{cases} \qquad \delta z^* = \begin{cases} -h_j & \text{if } \Delta z_b < 0 \text{ and } z_{sj} < z_{bi} \\ h_i & \text{if } \Delta z_b \geq 0 \text{ and } z_{si} < z_{bj} \\ \Delta z_b & \text{otherwise} \end{cases} \tag{52}$$

- Differential approximation:

$$\widetilde{H}^{dif} = -g_\psi \, \widetilde{h} \, \Delta z_b \tag{53}$$

The mass flux at the $\hat{x} = 0$ position satisfies the conservative condition $(q_n)_k^{\downarrow -} = (q_n)_k^{\downarrow +} = q_n^{\downarrow}$. Furthermore, we compute the characteristic frictionless mass flux q_n^* for the kth cell edge as

$$\begin{array}{ll} q_n^* = (hu_n)_i + \widetilde{\alpha}_1 \widetilde{\lambda}_1 - \widetilde{\beta}_{b1} & \text{if subcritical } \widetilde{\lambda}_2 > 0 \text{ or supercritical } \widetilde{\lambda}_3 < 0 \\ q_n^* = (hu_n)_j - \widetilde{\alpha}_3 \widetilde{\lambda}_3 + \widetilde{\beta}_{b3} & \text{if subcritical } \widetilde{\lambda}_2 < 0 \text{ or supercritical } \widetilde{\lambda}_1 > 0 \end{array} \tag{54}$$

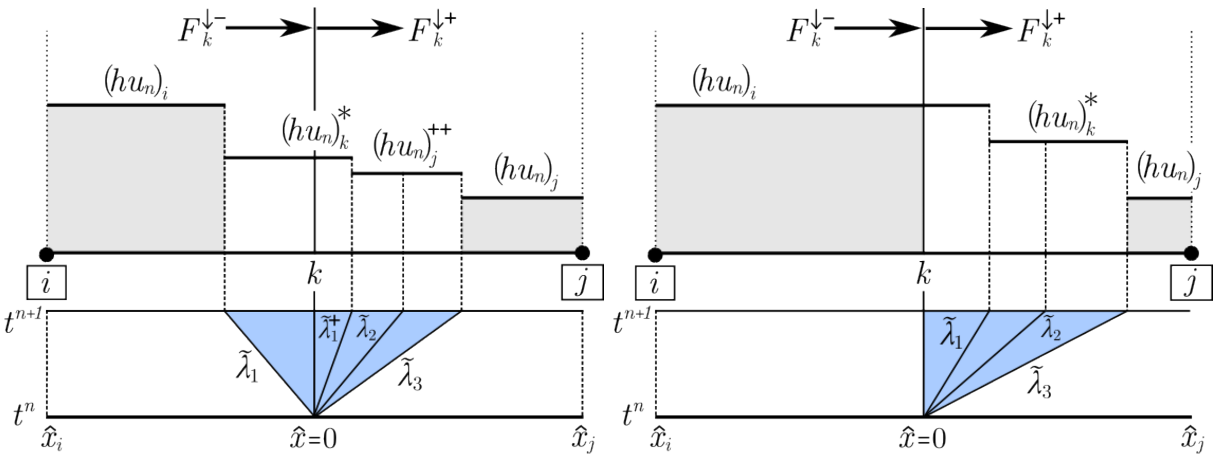

Figure 4: Inner states for the normal mass flux in edges with right-direction subcritical flow.

2.5. Basal resistance momentum contribution

The basal resistance contribution $\widetilde{T}_k$ at the kth cell edge in (39) should be opposite to the discharge and is hence defined as

$$\widetilde{T}_k = \begin{cases} -\text{sgn}\left(q_n^*\right) \, g_\psi \widetilde{h} \, \dfrac{\widetilde{n}_b^2 \, \widetilde{\mathrm{U}}^2}{h_{max}^{4/3}} \, d_{int} & \text{default} \\ 0 & \text{if } q_n^* = 0 \end{cases} \tag{55}$$

where the averaged Manning factor is $\widetilde{n}_b = \frac{1}{2}(n_{bi}+n_{bj})$, the characteristic velocity modulus is $\widetilde{\mathrm{U}} = \frac{1}{2}(|\mathbf{u}_i| + |\mathbf{u}_j|)$, the characteristic flow depth is $h_{max} = \max(h_i, h_j)$, and $\text{sgn}\left(q_n^*\right)$ denotes the direction of the frictionless discharge throughout the edge. The term d_{int} is the friction integration distance, calculated as

$$d_{int} = \begin{cases} |\widetilde{n}_{ux} \Delta x + \widetilde{n}_{uy} \Delta y| & \text{default} \\ d_{norm} & \text{if } \mathrm{U}_m < 1\mathrm{e}-3 \end{cases} \tag{56}$$

being $(\widetilde{n}_{ux}, \widetilde{n}_{uy})_k$ the components of the unity vector of the flow direction at the kth edge in the global framework, calculated as

$$\widetilde{n}_{ux} = \frac{1}{2}\left(\frac{u_i}{|\mathbf{u}_i|} + \frac{u_j}{|\mathbf{u}_j|}\right) \qquad \widetilde{n}_{uy} = \frac{1}{2}\left(\frac{v_i}{|\mathbf{u}_i|} + \frac{v_j}{|\mathbf{u}_j|}\right) \tag{57}$$

3. Explicit integration of momentum source terms

The correct integration of the momentum source terms $\mathbf{H}_k$ (36a) and $\mathbf{T}_k$ (36b) for the local plane RP associated to the kth cell edge ensures the well-balanced property of the augmented Riemann solver [10]. This well-balanced character ensures equilibrium in quiescent and steady states, as well as avoids numerical oscillations in the solution when large momentum sources appear [11, 12].

3.1. F-limitation for the basal friction

The explicit integration of the basal resistance term $\mathbf{T}_k$ (36b) is not straight-forward and requires a careful treatment in order to avoid numerical instabilities and additional time step restrictions. These additional time step restrictions can lead to a marked increase of the computational time required by the model. The consequence is a reduction of the efficiency, regardless of how the scheme is implemented (programming language, parallel computing, available hardware, etc).

The friction momentum contribution $\mathbf{T}_k$ (36b) in the local plane RP at the intercell edge is defined as

$$\mathbf{T}_k = \begin{pmatrix} 0 \\ \widetilde{T}_k \\ 0 \end{pmatrix} \tag{58}$$

and the source strengths linked to the basal friction are expressed as

$$\begin{aligned} \widetilde{\beta}_{\tau 1} &= \frac{-\widetilde{T}_k}{2\,\widetilde{c}_k} \\ \widetilde{\beta}_{\tau 2} &= 0 \\ \widetilde{\beta}_{\tau 3} &= \frac{\widetilde{T}_k}{2\,\widetilde{c}_k} \end{aligned} \tag{59}$$

We can always compute the characteristic mass flux including friction $(q_n)_k^{\downarrow -} = (q_n)_k^{\downarrow +} = q_n^{\downarrow}$ for the kth cell edge as

*** Quitar el condicional de regimen el codigo (water.cu)***

$$q_n^{\downarrow} = q_n^* - \widetilde{\beta}_{\tau 1} \tag{60}$$

Note that this expression (60) can be directly applied regardless of the flow direction and subcritical/supercritical regime occurs, since differences in the wave configuration are actually included in the characteristic frictionless mass flux q_n^* computation. Physically, the basal resistance term should always act slowing down the flow. Therefore, we define the following limitation for the resistance source strengths

$$\begin{aligned} \widetilde{\beta}_{\tau 1} &= \begin{cases} -\widetilde{T}_k/(2\,\widetilde{c}) & \text{default} \\ q_n^* & \text{if } q_n^{\downarrow}\, q_n^* \leq 0 \end{cases} \\ \widetilde{\beta}_{\tau 3} &= -\widetilde{\beta}_{\tau 1} \end{aligned} \tag{61}$$

Additionally, the friction source term is limited by a kinematic condition. We impose that momentum dissipated at the intercell edge due to the basal friction term should be in the same order of magnitude as the averaged kinematic energy at the edge, so

$$\frac{|\widetilde{T}_k|}{g_\psi\, \widetilde{h}} \leq \mathcal{O}\left(\frac{\widetilde{\mathrm{U}}\, |u_n|}{2\, g_\psi}\right) \tag{62}$$

3.2. P-correction for the flow depth

The momentum source integration can lead to unphysical values of the cell-averaged flow depth in subcritical wet-wet edges and requires a numerical fix. The P-corrention enforces non-negative values of the flow depth for the intermediate states at both sides of the intercell edge.

Only in **wet-wet subcritical walls**, i.e. $(\widetilde{\lambda}_1)_k < 0$ & $(\widetilde{\lambda}_3)_k > 0$, the convective intermediate state for the flow depth h^* at both sides of the edge, including the entropy-fix extra wave, can be calculated as

$$h_i^* = h_i^n + \widetilde{\alpha}_1 - \frac{\widetilde{\lambda}_3^-}{\widetilde{\lambda}_1}\widetilde{\alpha}_3 \tag{63a}$$

$$h_j^* = h_j^n - \widetilde{\alpha}_3 + \frac{\widetilde{\lambda}_1^+}{\widetilde{\lambda}_3}\widetilde{\alpha}_1 \tag{63b}$$

and the augmented intermediate states for the flow depth at the left and right side of the edge, h_i^- and h_j^+ respectively, must satisfy

$$h_i^- = h_i^* - \frac{\widetilde{\beta}_1}{\widetilde{\lambda}_1} \geq 0 \tag{64a}$$

$$h_j^+ = h_j^* + \frac{\widetilde{\beta}_3}{\widetilde{\lambda}_3} \geq 0 \tag{64b}$$

This limitation leads to a unique suitability range for the value of the momentum source strength $\widetilde{\beta}_1$ which ensures positivity for the intermediate states of h at both sides of the edge, imposed as

$$\widetilde{\beta}_1 \begin{cases} \geq \widetilde{\lambda}_1\, h_i^* & \text{Lower-limit} \\ \leq \widetilde{\lambda}_3\, h_j^* & \text{Upper-limit} \end{cases} \tag{65a}$$

$$\widetilde{\beta}_3 = -\widetilde{\beta}_1 \tag{65b}$$

4. Wet-dry front treatment

Tracking wet-dry fronts is one of the most challenging issues when computing realistic cases. We apply a four-step procedure to avoid numerical issues in wet-dry fronts:

1. Within the edge-contribution calculation loop, at wet-dry fronts, we set the no-reflective-wall condition if the flow depth inner state at the dry-cell, i.e. h_i^- and h_j^+ for left and right dry-cells respectively, is negative:

$$\begin{array}{c} \text{Right dry-cell} \\ h_i^n \geq 10^{-12} \\ \& \\ h_j^n < 10^{-12} \end{array} \begin{cases} h_j^+ = h_j^n - \widetilde{\alpha}_3 + \frac{\widetilde{\beta}_3}{\widetilde{\lambda}_3} < 0 & \begin{array}{l} \text{Right solid-wall cond. } \& \\ \left[\begin{array}{l} (\delta q_n)_k^{\downarrow -} = \sum\limits_{w=1}^{3} \left(\widetilde{\lambda}_w \widetilde{\alpha}_w - \widetilde{\beta}_w\right)_k \\ (\delta m_n)_k^{\downarrow -} = 0 \\ (\delta m_t)_k^{\downarrow -} = 0 \end{array} \right] \end{array} \\ \text{otherwise} & \text{Normal wall} \end{cases} \tag{66}$$

$$\begin{array}{c} \text{Left dry-cell} \\ h_i^n < 10^{-12} \\ \& \\ h_j^n \geq 10^{-12} \end{array} \begin{cases} h_i^- = h_i^n + \widetilde{\alpha}_1 - \frac{\widetilde{\beta}_1}{\widetilde{\lambda}_1} < 0 & \begin{array}{l} \text{Left solid-wall cond. } \& \\ \left[\begin{array}{l} (\delta q_n)_k^{\downarrow +} = \sum\limits_{w=1}^{3} \left(\widetilde{\lambda}_w \widetilde{\alpha}_w - \widetilde{\beta}_w\right)_k \\ (\delta m_n)_k^{\downarrow +} = 0 \\ (\delta m_t)_k^{\downarrow +} = 0 \end{array} \right] \end{array} \\ \text{otherwise} & \text{Normal wall} \end{cases} \tag{67}$$

*** Cambiar el calculo del inner h state, sacando la onda de correcion de la entropia ***

2. Within the cell updating loop, we set null $x-$ and $y-$momentum for cells with flow depth h_i^n lower than an user-defined threshold, refereed to as minimum-depth h_{min}:

$$\begin{array}{c} \text{Minimum-depth cells} \\ h_i^n < h_{min} \end{array} \begin{cases} (hu)_i^n = 0 \\ (hv)_i^n = 0 \end{cases} \tag{68}$$

3. At wet-dry fronts, we identify each wet-dry edge with a upward bed level step higher than the flow depth in the wet-cell and we also set solid-wall condition at these edges:

$$\begin{array}{c} \text{Left dry-cell} \\ h_i^n < 10^{-12} \\ \& \\ h_j^n \geq 10^{-12} \end{array} \begin{cases} (z_b)_i^n > (z_b + h)_j^n & \text{Left solid-wall cond.} \\ \text{otherwise} & \text{Normal wall} \end{cases} \tag{69}$$

$$\begin{array}{c} \text{Right dry-cell} \\ h_i^n \geq 10^{-12} \\ \& \\ h_j^n < 10^{-12} \end{array} \quad \begin{cases} (z_b + h)_i^n < (z_b)_j^n & \text{Right solid-wall cond.} \\ \text{otherwise} & \text{Normal wall} \end{cases} \tag{70}$$

4. Finally, within a specific cell loop, we set null normal momentum at wet-cells for each edge with solid-wall condition or closed boundary condition, as:

$$\begin{array}{c} \text{Solid-wall cond.} \\ || \\ \text{Closed boundary cond.} \end{array} \quad \begin{cases} (hu)_i^n = (hu)_i^n - q_{ni}\, n_x \\ (hv)_i^n = (hv)_i^n - q_{ni}\, n_y \\ \\ \text{ with } q_{ni} = (hu)_i^n\, n_x + (hv)_i^n\, n_y \end{cases} \tag{71}$$

References

References

[1] C. Juez, J. Murillo, P. García-Navarro, 2d simulation of granular flow over irregular steep slopes using global and local coordinates, J. Comput. Phys 255 (2013) 166–204.

[2] E. Godlewski, P.-A. Raviart, Numerical Approximation of Hyperbolic Systems of Conservation Laws, Springer-Verlag, New York, 1996.

[3] E. Toro, Riemann Solvers and Numerical Methods for Fluid Dynamics: A Practical Introduction, Springer-Verlag, Berlin, Germany, 1997.

[4] J. Murillo, P. García-Navarro, Weak solutions for partial differential equations with source terms: application to the shallow water equations, J. Comput. Phys 229 (2010) 4327–4368.

[5] M. Castro, E. Fernández-Nieto, A. Ferreiro, J. García-Rodríguez, C. Parés, High order extensions of roe schemes for two-dimensional nonconservative hyperbolic systems, Journal of Scientific Computing 39 (2009) 67–114.

[6] J. Murillo, P. García-Navarro, Energy balance numerical schemes for shallow water equations with discontinuous topography, J. Comput. Phys 236 (2012) 119–142.

[7] G. Rosatti, L. Begnudelli, The Riemann problem for the one-dimensional, free-surface shallow water equations with a bed step: theoretical analysis and numerical simulations, J. Comput. Phys 229 (2010) 760–787.

[8] J. Li, G. Chen, The generalized riemann problem method for the shallow water equations with bottom topography, Int J. Numer. Meth. Eng 65 (2006) 834–862.

[9] A. Harten, J. Hyman, Self adjusting grid methods for one-dimensional hyperbolic conservation laws, Journal of Computational Physics 50 (1983) 235 – 269.

[10] J. Murillo, A. Navas-Montilla, A comprehensive explanation and exercise of the source terms in hyperbolic systems using Roe type solutions. application to the 1D-2D shallow water equations, Advances in Water Resources 98 (2016) 70 – 96.

[11] J. Burguete, P. García-Navarro, J. Murillo, Friction term discretization and limitation to preserve stability and conservation in the 1d shallow-water model: Application to unsteady irrigation and river flow, Int. J. Numer. Meth. Fluids 54 (2008) 403–425.

[12] J. Murillo, P. García-Navarro, J. Burguete, Time step restrictions for well balanced shallow water solutions in non-zero velocity steady states, Int. J. Numer. Meth. Fluids 56 (2008) 661–686.

[13] F. Z. Leighton, A. G. L. Borthwick, P. H. Taylor, 1-d numerical modelling of shallow flows with variable horizontal density, International Journal for Numerical Methods in Fluids 62 (2010) 1209–1231.

[14] S. Martínez-Aranda, J. Murillo, P. García-Navarro, A new 2D bedload transport model based on non-capacity approach to overcome the problems associated to finite-depth sediment layers, in: In proceedings of the 10th International Conference on Fluvial Hydraulics (River Flow 2020), July 7-10, Delft, Netherlands, 2020.